

Fatjet Signatures of Quintuplet Fermions at the LHC

^aSourabh Dube¹, ^bNilanjana Kumar², ^aShriyansh Ranjan³

^a*Indian Institute of Science Education and Research (IISER), Pune, India*

^b*Department of Physics, Chettinad Institute of Technology, Chettinad Academy of Research and Education, Tamilnadu 603103, India*

Abstract

This paper explores a simplified extension of the standard model featuring a neutral fermion quintuplet and a scalar quadruplet, which together generate neutrino masses through tree and loop level mechanisms. The quintuplet fermions decay into standard model gauge bosons via the scalars, producing unique collider signatures at the LHC characterized by multilepton and multijet final states. The study focuses on the pair production of quintuplet fermions in the 700–1200 GeV mass range, where their decays produce highly boosted W and Z bosons identifiable as *fatjets*. Emphasis is placed on the production and decay of doubly charged fermions due to their higher cross section. Advanced jet substructure and kinematic techniques are applied to enhance sensitivity by reducing standard model backgrounds. A detailed analysis of signal significance is performed in the two lepton, two fatjet (2L2F_j) and three lepton, one fatjet (3L1F_j) channels for different masses of the fermion and the scalars, optimizing selection cuts to maximize signal efficiency over standard model backgrounds. The study found that both channels exhibit excellent performance, with significance exceeding 5σ under realistic conditions including a 50% background uncertainty at integrated luminosities up to 3000 fb⁻¹.

1 Introduction

The standard model (SM) of particle physics, though highly successful, cannot explain several observed phenomena such as the small neutrino masses [1], the particle nature of dark matter, the muon anomalous magnetic moment [2], and certain flavor anomalies [3] among many others. Extensions of the SM introduce physics at or beyond the TeV scale to address the shortcomings of the SM. Some popular examples are extensions of the SM with vector-like quarks and leptons [4–6], fermion multiplets [7–9] or scalar multiplets [10–12]. Beyond SM scenarios featuring both fermion and scalar multiplets, including cases with more than one set of new multiplets, have been widely studied in the literature. The appearance of both fermion and scalar multiplets is natural in models of grand unified theories [13], Left-Right Symmetric scenarios [14, 15], Little Higgs [16], and Composite Higgs Models [17]. Additionally, models such as the minimal R ν MDM [18] incorporate a scalar or fermionic quintuplet and a vector-like quadruplet fermion for unified explanations of neutrino mass and dark matter candidates.

In general, models with more than one multiplet or one type of BSM particle often allow interaction among themselves which results in distinct decay modes and thus the collider signatures are unique. The mass difference between different BSM multiplets or particles plays a crucial role in the kinematics. These models have gained a lot of interest recently. If we denote by X and Y the different BSM particles, then for example, in Ref [19] X and Y are leptoquark and vector-like leptons. In Ref [20] X and Y are two leptonic multiplets belonging to different $SU(2)_L$. In composite Higgs models [21, 22], X

¹sdube@iiserpune.ac.in

²nilanjana.kumar@gmail.com

³shriyanshranjan1@gmail.com

and Y can be two different pNGB scalars or one pNGB scalar and one heavy resonance. In this paper, we examine a model with a neutral fermion quintuplet (with zero hypercharge) and a scalar quadruplet; which allows for neutrino mass generation via tree-level and loop-level mechanisms [8, 9, 23].

We choose a scenario where only one scalar quartet (ϕ_4) and one quintuplet fermion (Σ_R) is present. This model provides a unique signature at the LHC and future collider experiments [24] in multilepton and multijet final states. Once produced at the LHC, these quintuplet fermions decay to SM gauge bosons via the scalars where the fermions are heavier than the scalars. It was shown in Ref [9] that the final states with lepton and jets suffer from very small cross sections, especially when the mass of the fermion quintuplet is around 1 TeV.

Current searches for the exotic fermions and scalars have put strong bounds on their masses. For example, the ATLAS experiment sets a lower limit on fermion mass of 910 GeV [25]. The CMS experiment sets constraints on the fermion masses for varied coupling scenarios, with the lower limit being as high as 1065 GeV [26] in specific cases. The direct search limit on charged Higgs bosons of 80 GeV comes from the LEP experiments [27]. Both ATLAS and CMS have conducted extensive searches targeting multiple production and decay modes of the scalars. A lower limit of ~ 200 GeV is placed on the masses of charged scalars from various channels, when the scalars decay to the SM gauge bosons [28–30]. Limits exist on the production cross section of the charged scalars when they decay to SM fermions [31, 32]. These searches have placed a stricter lower limit on the charged Higgs mass of ~ 400 GeV. The LHC limits are not directly applicable on the model under study since the quintuplet fermions decay through scalars. However, to analyze the fatjet signatures we consider the mass of the fermion quintuplet ≥ 700 GeV, and the mass of the scalar multiplet at ≥ 600 GeV, which is above the current lower bounds.

Standard searches for fermion multiplets are proposed widely in the literature [33–38]. In this paper we investigate the pair production of the quintuplet fermions where the fermions decay via the charged scalars to the SM gauge bosons. If the mass of the fermion multiplet is ≥ 700 GeV, then the W/Z bosons from the decay of the scalars are expected to be highly boosted and they can be identified as *fatjets*. Fatjets are the resultant objects of jet clustering algorithms using a large radius parameter, thus making them *fat*. Fatjet searches at the LHC have become a critical tool for probing BSM particles. Fatjet signatures are studied in various BSM models with fermion multiplets to achieve sensitivity to masses up to and beyond TeV scale [39–41]. Here we primarily focus on the production of the doubly charged fermions because of its higher production cross section as compared to the other pair production modes. We show that advanced jet reconstruction and jet substructure [42] techniques help to suppress SM backgrounds and enhance the sensitivity of LHC experiments.

2 The Model

We consider a simplified model where the SM is extended with a quintuplet fermion (Σ_R) and a quartet scalar (ϕ_4). This model has been studied previously in detail [8, 9, 24]. The quintuplet fermion Σ_R of hypercharge 0 can be expressed as, $\Sigma_R \equiv [\Sigma_1^{++}, \Sigma_1^+, \Sigma^0, \Sigma_2^-, \Sigma_2^{--}]^T_R$ and the scalar multiplets with hypercharge $1/2$ is given by, $\Phi_4 = (\varphi^{++}, \varphi_2^+, \varphi^0, \varphi_1^-)^T$. The gauge coupling of Σ_R is obtained as,

$$\mathcal{L}_{gauge, \Sigma} \supset (eA_\mu + gc_w Z_\mu) \left[2(\bar{\Sigma}_R^{++} \gamma^\mu \Sigma_R^{++} + \bar{\Sigma}_L^{++} \gamma^\mu \Sigma_L^{++}) + \bar{\Sigma}_R^+ \gamma^\mu \Sigma_R^+ + \bar{\Sigma}_L^+ \gamma^\mu \Sigma_L^+ \right] - \quad (1)$$

$$g \left\{ \left[\sqrt{2}(\bar{\Sigma}_R^+ \gamma^\mu \Sigma_R^{++} - \bar{\Sigma}_L^+ \gamma^\mu \Sigma_L^{++}) + \sqrt{3}(\bar{\Sigma}_R^0 \gamma^\mu \Sigma_R^+ - \bar{(\Sigma_R^0)}^C \gamma^\mu \Sigma_L^+) \right] W_\mu^- + h.c. \right\} \quad (2)$$

The interaction of the quartet scalar with the gauge bosons is obtained from the kinetic term as

$$\mathcal{L}_{gauge,\Sigma} \supset \frac{\sqrt{3}}{2} \frac{g^2}{cw} v_4 (2 - s_W^2) W_\mu^+ Z^\mu \phi_1^- + \frac{g^2}{cw} v_4 s_W^2 W_\mu^+ Z^\mu \phi_2^- \quad (3)$$

$$+ \sqrt{\frac{3}{2}} g^2 v_4 W_\mu^+ W^{+\mu} \phi^{--} + h.c. \quad (4)$$

The scalar also couples with the quintuplet fermion via the Yukawa term.

$$-\mathcal{L}_{yuk} \supset (y_\nu)_{ij} [\bar{L}_{L_i} \tilde{\Phi}_4 \Sigma_{R_j}] + h.c. \quad (5)$$

Upon expansion,

$$-\mathcal{L}_{yuk} = (y_\nu)_{ij} \left[\bar{\nu}_{L_i} \left(\Sigma_{1R_j}^{++} \varphi^{--} + \frac{\sqrt{3}}{2} \Sigma_{1R_j}^+ \varphi_1^- + \frac{1}{\sqrt{2}} \Sigma_{R_j}^0 \varphi_1^{0*} + \frac{1}{2} \Sigma_{2R_j}^- \varphi_2^+ \right) \right. \quad (6)$$

$$\left. + \bar{\ell}_{L_i} \left(\frac{1}{2} \Sigma_{1R_j}^+ \varphi^{--} + \frac{1}{\sqrt{2}} \Sigma_{R_j}^0 \varphi_1^- + \frac{\sqrt{3}}{2} \Sigma_{2R_j}^- \varphi_1^{0*} + \Sigma_{2R_j}^- \varphi_2^+ \right) \right] + h.c. \quad (7)$$

Here, we have neglected the mixing among the individual components of the multiplets and we choose the components of the quintuplet fermion as well as the scalar multiplets to be degenerate, which we denote as m_Σ and m_ϕ , respectively [8]. We also consider $m_\Sigma > m_\phi$, which is naturally implied from the muon anomalous magnetic moment measurement, as shown in [9]. For the complete Lagrangian we refer to Ref. [8].

The charged fermions Σ^\pm and $\Sigma^{\pm\pm}$ decay via the following modes:

$$\Sigma^\pm \rightarrow \phi_2(\phi_1)^\pm \nu(\bar{\nu}), \phi^{\pm\pm} l^\mp, \phi^0 l^\pm \quad (8)$$

$$\Sigma^{\pm\pm} \rightarrow \phi^{\pm\pm} \nu(\bar{\nu}), \phi_2^\pm l^\pm \quad (9)$$

where $l = e, \mu, \tau$. The branching ratios are $\Sigma^{\pm\pm} \rightarrow \phi^{\pm\pm} \nu(\bar{\nu}) = \Sigma^{\pm\pm} \rightarrow \phi_2^\pm l^\pm = 50\%$. The scalars further decay to SM gauge bosons with 100% branching ratio:

$$\begin{aligned} \phi_2^\pm(\phi_1^\pm) &\rightarrow W^\pm Z \\ \phi^{\pm\pm} &\rightarrow W^\pm W^\pm \\ \phi^0 &\rightarrow W^+ W^- \end{aligned} \quad (10)$$

3 Signal and Background at the LHC

The charged and neutral scalars can be pair produced at the LHC via photon and Z boson mediated Drell–Yan (DY) processes and also via a t -channel process. The cross section of $pp \rightarrow \Sigma^\pm \Sigma^\pm$ is significantly smaller than $pp \rightarrow \Sigma^{\pm\pm} \Sigma^{\mp\mp}$ because the production cross section varies with the fourth power of the charge. A detailed discussion of the pair production cross section is given in Ref. [24]. Here we investigate the pair production of $\Sigma^{\pm\pm} \Sigma^{\mp\mp}$ at pp collisions at the centre-of-mass energy of 14 TeV. The photon parton distribution function (PDF) for the proton is included to the initial state of the process given its significant contribution to the production cross section. The diagrams leading to the pair production of $\Sigma^{\pm\pm} \Sigma^{\mp\mp}$ are shown in Fig. 1 following the decays (one among many) of the particles.

The inclusion of the photon PDF [43] raises the question of the choice of PDF to use when generating simulation samples. To investigate this, we used different versions of NNPDF23 [44, 45]. We compare

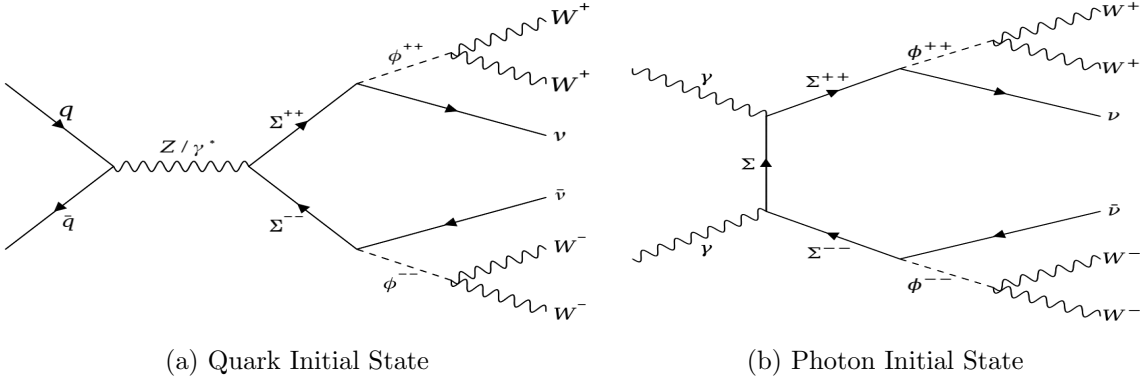


Figure 1: Feynman diagrams of the doubly charged fermion pair production at the LHC, where q stands for u, d, c, s, b quarks.

a quark-only initial state, a photon-only initial state, and an inclusive initial state using three different LO and NLO PDFs for two different masses of $\Sigma^{\pm\pm}$, 400 GeV and 1000 GeV. For this, MADGRAPH [46, 47] incorporated with LHAPDF [48] is used. We observe a significant increase in the production cross section by using a photon PDF for $m_{\Sigma} = 1000$ GeV, and modest increase at 400 GeV irrespective of the choice of PDFs. We use the cross section calculated by using NNPDF2.3QED at NLO, specifically NNPDF23_nlo_as_0119_qed, and show this in Table 1. The increase in the production cross section after including the photon PDF is also shown and the uncertainties in the cross sections are found to be $< 1\%$.

$m_{\Sigma^{\pm\pm}}$ (GeV)	PDF used	Production cross section (pb)			Relative increase in cross section (%)
		quark-only	photon-only	inclusive	
400	NNPDF23_nlo_as_0119_qed	0.1851	0.0094	0.1944	5.0
1000	NNPDF23_nlo_as_0119_qed	0.001767	0.000327	0.002089	18.2

Table 1: Pair production cross section of $\Sigma^{++}\Sigma^{--}$ is compared for initial states that are quark-only, photon-only, and inclusive in 14 TeV pp collisions. The percentage increase in the inclusive case is calculated with respect to the quark-only initial state.

The different decays of the quintuplet fermions and the quadruplet scalars give rise to the following final states involving bosons and leptons.

$$pp \rightarrow \Sigma^{\pm\pm}\Sigma^{\mp\mp} \rightarrow \phi^{\pm\pm}\nu\phi^{\mp\mp}\bar{\nu} \rightarrow W^+W^+W^-W^- + \nu\bar{\nu} \quad (11)$$

$$pp \rightarrow \Sigma^{\pm\pm}\Sigma^{\mp\mp} \rightarrow \phi_2^{\pm}l^+\phi_2^{\mp}l^- \rightarrow W^+ZW^-Z + l^+l^- \quad (12)$$

$$pp \rightarrow \Sigma^{\pm\pm}\Sigma^{\mp\mp} \rightarrow \phi^{\pm\pm}\nu\phi_2^{\mp}l^- \rightarrow W^+W^-W^-Z + l^- + \nu \quad (13)$$

Three benchmark points for the signal are considered for the analysis:

- **Low-mass:** $m_{\Sigma^{++}} = 700$ GeV, $m_{\phi^{++}} = 600$ GeV
- **Med-mass:** $m_{\Sigma^{++}} = 1200$ GeV, $m_{\phi^{++}} = 600$ GeV
- **High-mass:** $m_{\Sigma^{++}} = 1200$ GeV, $m_{\phi^{++}} = 1100$ GeV

The W and Z bosons in the final state are often boosted when they decay hadronically, and thus can be identified as fatjets. The first channel can provide up to four W -fatjets whereas the second and third channel generate up to four fatjets which can be either W - or Z -fatjets. Although the expected production yield is identical for each channel, we opt for channel 1 – characterized by four W bosons. Having a single type of fatjet will streamline the analysis. Figure 1 shows the pair production process of the doubly charged fermion leading to four W 's in the final state.

The efficiency of reconstructing and identifying the W -fatjets increases when the mass of the parent particle is ~ 1 TeV since the W is boosted and the decay products of the W become increasingly collimated. At a hadron collider, the presence of a lepton in the final state allows a large reduction in the SM background. We combine the requirement of a W -fatjet and a lepton to maximize our advantage and choose to study the following two final states:

1. 2L2F_j: Two leptons ($L = e, \mu, \tau$) with two W -fatjets
2. 3L1F_j: Three leptons ($L = e, \mu, \tau$) with one W -fatjet

These final states ensure that we reduce the SM background significantly, while at the same time maintaining good efficiency for lower ϕ masses. Table 2 shows the cross section (σ) \times branching ratio (\mathcal{B}) for the three chosen benchmark points. We have assumed $\mathcal{B}(\Sigma^{++} \rightarrow \phi^{++} \nu) = 100\%$.

2L2F _j	$m_{\Sigma^{++}}, m_{\phi^{++}}$ (GeV)	$\sigma \times \mathcal{B}$ (pb)
	1200,1100 (high-mass)	1.455×10^{-4}
	1200,600 (med-mass)	1.455×10^{-4}
	700,600 (low-mass)	3.627×10^{-3}
3L1F _j	$m_{\Sigma^{++}}, m_{\phi^{++}}$ (GeV)	$\sigma \times \mathcal{B}$ (pb)
	1200,1100 (high-mass)	4.405×10^{-5}
	1200,600 (med-mass)	4.405×10^{-5}
	700,600 (low-mass)	1.098×10^{-3}

Table 2: The cross section \times branching ratio in the channels of interest for the three benchmark points.

Several SM processes can give rise to backgrounds in the 2L2F_j final state. The dominant contribution comes from $t\bar{t}Z$ [49] where the Z produces two leptons, and two W bosons along with b quarks originate from the top decay. Similarly, the ZVV [50] process, where V denotes a W or a Z , also contributes to the background. Due to the large cross section, $t\bar{t}$ [51] production with additional jets is also a source of background. This process contributes when the W bosons decay leptonically, and the jet arising from the b -quark is misidentified as a fatjet.

The possible backgrounds for the 3L1F_j final state are: WZ +jets [52, 53], $t\bar{t}Z$ [49], $t\bar{t}W$ [54] and $t\bar{t}$ +jets. The WZ +jets contributes the most when both of the bosons decay leptonically producing three leptons and the one of the jets is misidentified as a fatjet. In $t\bar{t}W$ process, the three leptons can arise from any of the W bosons, or from the semi-leptonic decays of b -hadrons, and any of the W 's can give rise to the fatjet. The requirement of three leptons makes the contribution from $t\bar{t}$ + jets negligible.

4 Analysis of Fatjet Signals at the LHC

Simulation for the signal and background processes at the LHC was done with MADGRAPH5_AMC@NLO [46] with PYTHIA 8.3 [55, 56] used for hadronization of the event. The anti- k_t jet clustering algorithm [57] as implemented in the FASTJET [58] package within the DELPHES [59] framework is used for clustering jets and fatjets. For the signal, 5×10^4 collision events are simulated for each benchmark point. For each of the $t\bar{t}Z$, $t\bar{t}W$, and $WZ+jets$ processes we generate 5×10^5 events. For $t\bar{t}+jets$ and ZVV processes, 1×10^6 and 2×10^6 events are produced respectively.

The initial object selections are as follows:

- Hadronically-decaying τ leptons (τ_h) are reconstructed from the visible daughter particles (i.e. excluding the neutrino). The visible daughter particles thus exclude electrons and muons. Only τ_h originating from a signal particle or a gauge boson are considered.
- Electrons and muons are also required to originate either from a signal particle or a gauge boson, or from a τ lepton which has originated from a signal particle or a gauge boson.
- We require $p_T(e, \mu) > 10$ GeV, $|\eta(e, \mu)| < 2.4$ $p_T(\tau_h) > 20$ GeV, $|\eta(\tau_h)| < 2.3$. The leading lepton in the event is required to satisfy $p_T > 30$ GeV to mimic a trigger requirement.
- Regular jets are clustered with the jet radius parameter $R = 0.5$ and must satisfy $p_T > 30$ GeV and $|\eta| < 2.4$.
- Fatjets are clustered with $R = 0.8$ and must satisfy $p_T > 200$ GeV and $|\eta| < 2.4$.
- Regular and fatjets are required to be away from the selected leptons by imposing $\Delta R(lj) > 0.4$, where $\Delta R = \sqrt{(\Delta\eta_{lj})^2 + (\Delta\phi_{lj})^2}$.

4.1 Kinematic Variables

The signal and background events can be discriminated by using additional kinematic variables. These are defined below:

- p_T^{miss} : defined as the magnitude of the vector sum of transverse momenta of all the observed particles in the event – $p_T^{\text{miss}} = \left| \sum_{i=\text{observed}} \vec{p}_T^i \right|$
- L_T : defined as the scalar sum of p_T of all the charged leptons that constitute the final state – $L_T = \sum_{i=\text{leptons}} p_T^i$
- H_T : defined as the scalar sum of p_T of all the regular jets – $H_T = \sum_{i=\text{jets}} p_T^i$
- S_T : defined as the sum of L_T , H_T and p_T^{miss} – $S_T = L_T + H_T + p_T^{\text{miss}}$
- m_{min} : defined as the minimum of all of the invariant masses of lepton pairs, irrespective of their charge or flavor.
- dR_{min} : defined as the minimum of all of the angular distances between lepton pairs in the event.

- Jet momentum fraction (*JMF*): defined as the ratio of the scalar sum of p_T of the fatjets to the H_T –

$$JMF = \frac{\sum_{i=\text{fatjets}} p_T^i}{H_T}$$

Aside from these quantities, the analysis uses several jet substructure variables to select the desired fatjets.

Jet Grooming: Since fatjets are considerably wider than regular jets, radiation from the underlying event or pileup can cause an overestimation of the fatjet invariant mass and degrade the mass resolution. Jet grooming algorithms are applied to the fatjets to account for these effects by removing unwanted soft radiation. There are two algorithms of jet grooming that we consider: the soft drop algorithm [60] and the jet pruning algorithm [61]. To compare these two, the resulting fatjet mass and p_T after grooming is examined for the low-mass benchmark point and shown in Fig. 2 (left). We find that the performance of the two algorithms is very similar. We choose the soft drop algorithm, as the peak of the jet mass distribution is closer to m_W , and the jet p_T is slightly higher.

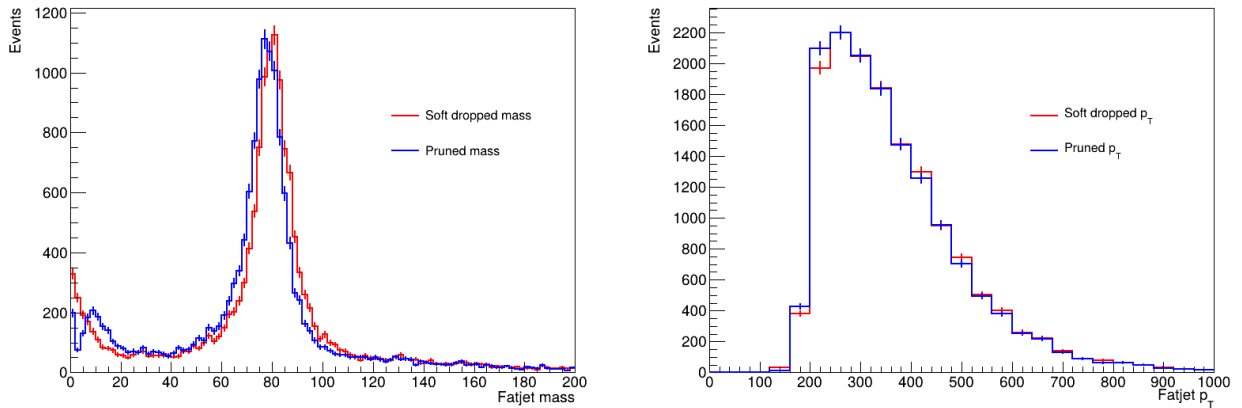


Figure 2: Jet mass (left) and p_T (right) of the leading fatjet for two different jet grooming algorithms: soft drop and jet pruning. The low-mass benchmark point is used here.

n-subjettiness: The n-subjettiness variables (τ_n) [62] can be used by taking ratios of subsequent n-subjettiness ($\tau_{p(p-1)} = \tau_p / \tau_{p-1}$) to obtain a relative probability of the jet being p -pronged or $(p-1)$ -pronged. Figure 3 (left) shows the behavior of τ_{21} and τ_{32} for the low-mass and high-mass benchmark points. The low value of τ_{21} and high value τ_{32} show that the W -fatjet has a 2-prong nature.

Relative Mass The relative mass (ρ) of a fatjet is calculated using the the soft drop mass (m_{SD}) and jet p_T as $\rho = 2 \ln(m_{SD}/p_T)$. This helps avoid regions where non-perturbative effects lead to discrepancies in generator predictions [63]. Figure 3 (right) shows the behavior of the ρ variable of the leading fatjet for the low-mass and high-mass benchmark points. We see that the non-perturbative effects are less significant for the high-mass point.

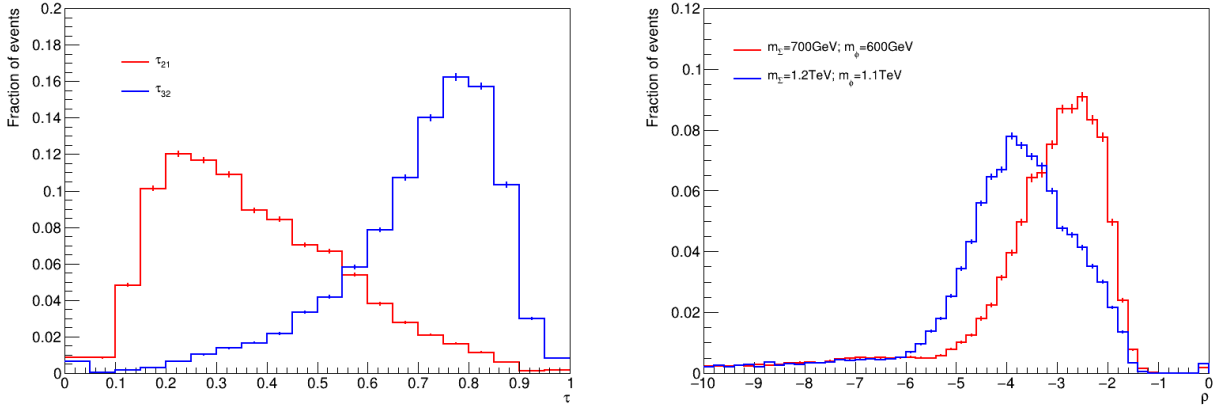


Figure 3: The τ_{21} and τ_{32} variables (left) for the leading fatjets in the low-mass benchmark point and the relative mass ρ (right) for the leading fatjets in the low-mass and high-mass benchmark points.

4.2 2L2F_j Channel

The 2L2F_j final state arises from the process $pp \rightarrow \Sigma^{++}\Sigma^{--} \rightarrow \phi^{++}\nu\phi^{--}\bar{\nu} \rightarrow W^+W^+\nu W^-W^-\bar{\nu}$ when two of the four W bosons decay leptonically and the other two decay hadronically. In Fig. 4 we show the distribution of p_T of the leading and subleading lepton and fatjet, and the p_T^{miss} in signal events. As expected, the high-mass signal benchmark point shows larger values of each of these variables.

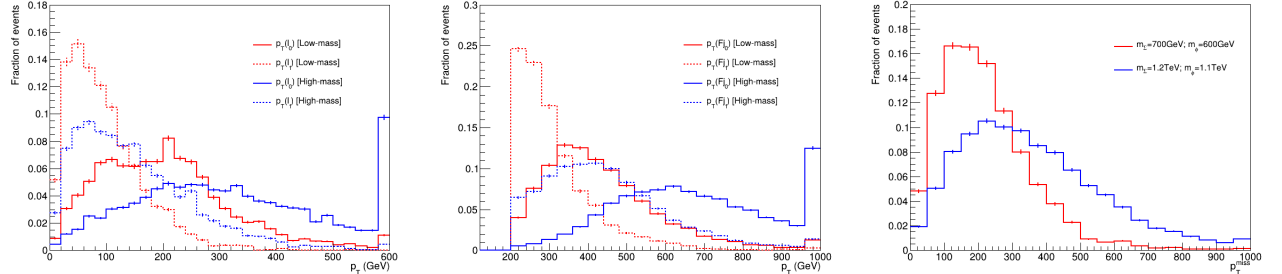


Figure 4: The p_T of the leading and subleading lepton (left), p_T of the leading and subleading fatjet (middle), and p_T^{miss} (right) are shown for the low-mass and high-mass benchmark points. The distributions in each figure are normalized to have unit area.

The event selection is applied in three sequential stages: **S1** is applied to all signal benchmark points, **S2** is applied differently for the three benchmark scenarios, and **S3** is applied to the fatjets:

- S1: We require events to satisfy $p_T^{\text{miss}} > 50$ GeV, $m_{\text{min}} > 50$ GeV, $H_T > 200$ GeV, $S_T > 500$ GeV, and $L_T + p_T^{\text{miss}} > 100$ GeV. The distributions of some kinematic variables after passing S1 are shown in Fig. 5.
- S2: We require $m_{\text{min}} > 100$ GeV, $dR_{\text{min}} > 1.0$, and $0.7 < JMF < 1.1$ for all events. Additional selections are imposed on H_T , L_T , S_T , and $L_T + p_T^{\text{miss}}$, which are summarized in Table 3. The $L_T + p_T^{\text{miss}}$ requirement is effective at suppressing the $t\bar{t}$ background for the low- and mid-mass points.

- S3: We require the selected fatjets to satisfy $60 < m_{SD} < 100$ GeV, $\tau_{21} < 0.8$, $\tau_{32} > 0.3$, and $\rho > -5.5$. The distributions of these variables after S2 are shown in Fig. 6.

The cut-flow is shown in Table 5.

S2	H_T	L_T	$L_T + p_T^{\text{miss}}$	S_T
low-mass	>500	>100	>300	>1100
mid-mass	>500	>100	>500	>1400
high-mass	>700	> 200	>500	>1400

Table 3: The selections implemented in S2 for the signal and background processes in the 2L2F_j final state. The selections are shown in units of GeV.

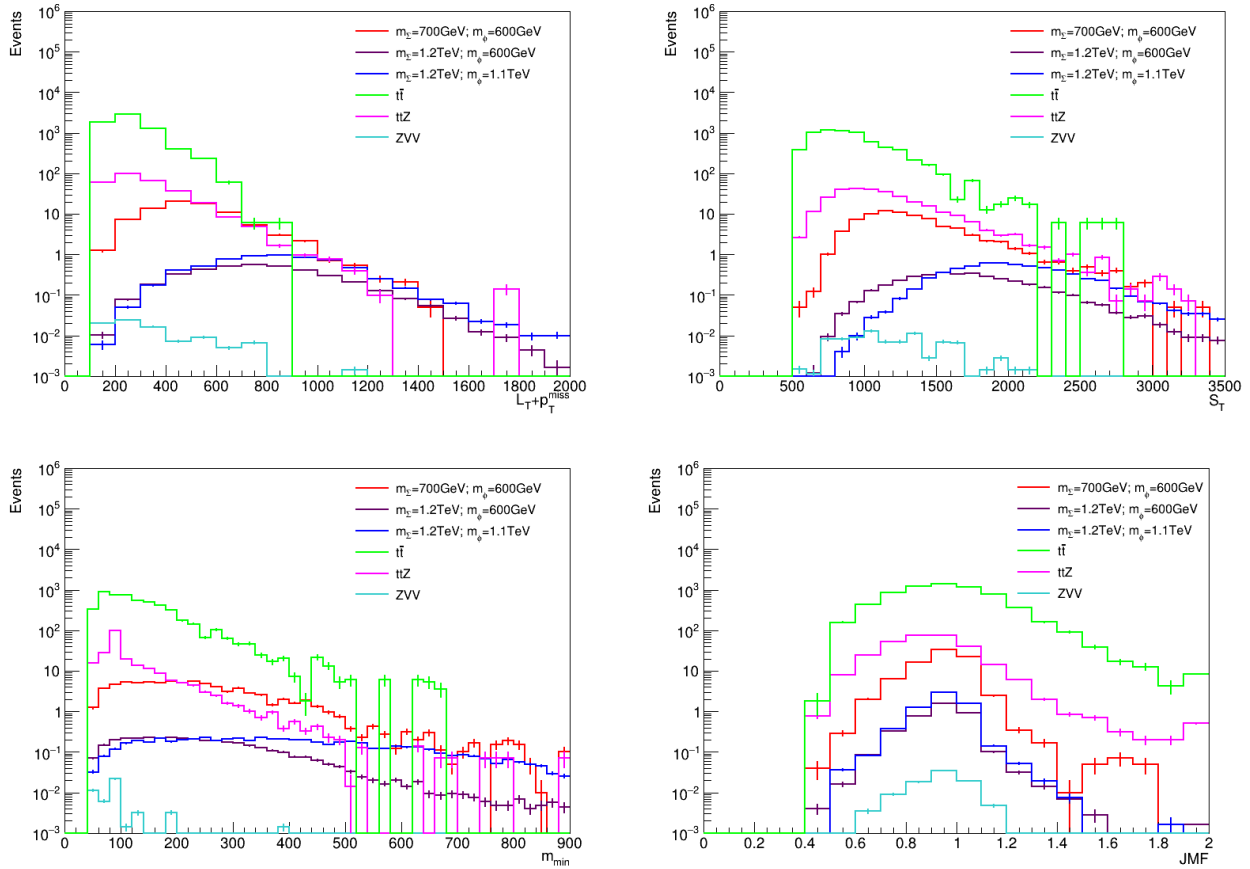


Figure 5: The distributions of $L_T + p_T^{\text{miss}}$, S_T (top row) and m_{min} , JMF (bottom row) are shown for signal and background processes after the S1 selections are imposed in the 2L2F_j final state.

4.3 3L1F_j Channel

The 3L1F_j final state arises from the process $pp \rightarrow \Sigma^{++}\Sigma^{--} \rightarrow \phi^{++}\nu\phi^{--}\bar{\nu} \rightarrow W^+W^+\nu W^-W^-\bar{\nu}$ when one of the W bosons decays hadronically, and all others decay leptonically. As in the case of 2L2F_j, here as well we apply the event selection in three sequential stages, S1, S2, and S3.

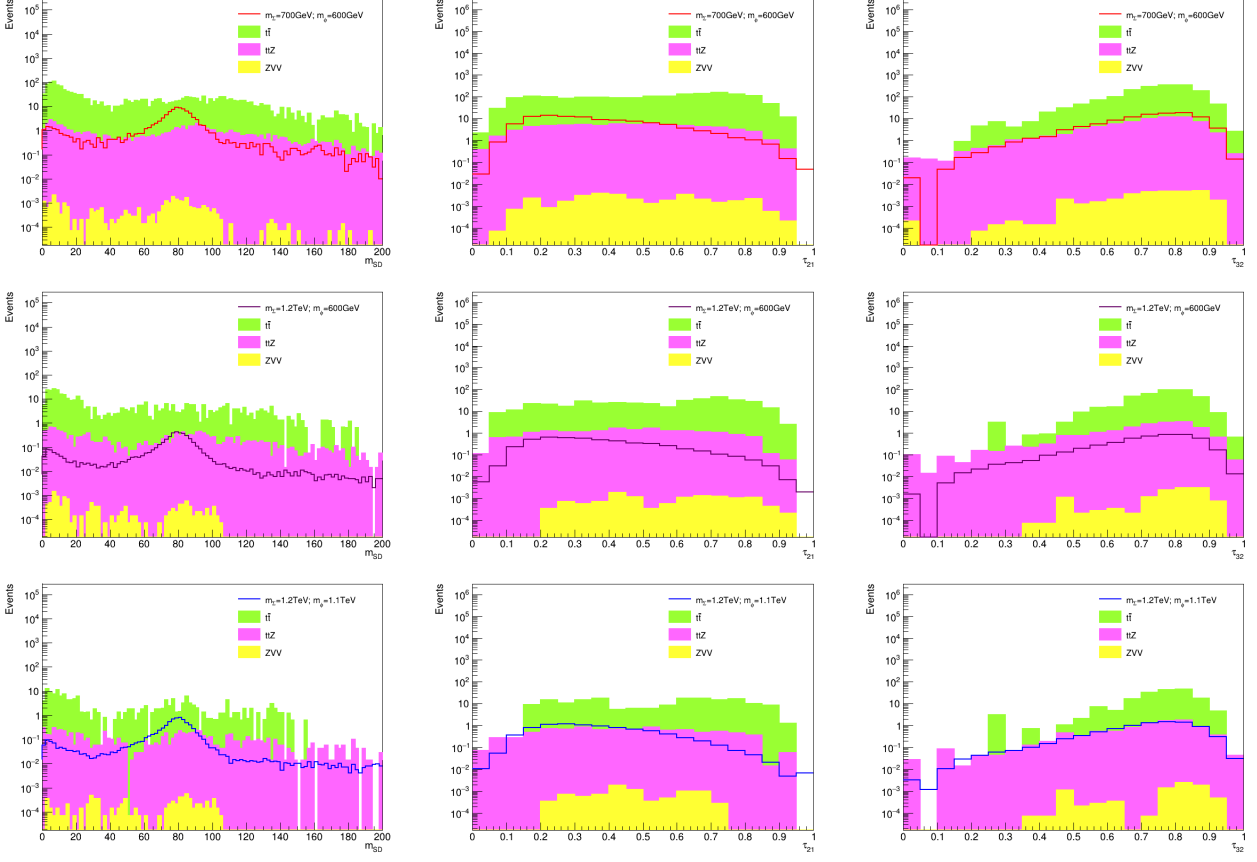


Figure 6: The jet substructure variables for the low-mass (top), med-mass (middle), and high-mass (bottom) benchmark point and the background processes after the S2 selections are imposed in the 2L2F_j final state.

- S1: We require events to satisfy $p_T^{\text{miss}} > 50$ GeV, $m_{min} > 50$ GeV, $H_T > 200$ GeV, $S_T > 400$ GeV, and $L_T + p_T^{\text{miss}} > 200$ GeV. The distributions of some kinematic variables after passing S1 are shown in Fig. 7. These follow a similar pattern as that in the 2L2F_j final state. In this channel however, the smaller number of fatjets, and larger number of leptons requires changes to the H_T and L_T selections.
- S2: We require $m_{min} > 100$ GeV, $dR_{min} > 1.0$, and $0.7 < JMF < 1.1$ for all events. Additional selections are imposed on H_T , L_T , S_T , and $L_T + p_T^{\text{miss}}$, which are summarized in Table 4.
- S3: We require the selected fatjet to satisfy $60 < m_{SD} < 100$ GeV, $\tau_{21} < 0.8$, $\tau_{32} > 0.3$, and $\rho > -5.5$. The distributions of these variables after S2 are shown in Fig. 8.

The cut-flow is shown in Table 5.

4.4 Results

We now summarize the results for the 2L2F_j and 3L1F_j channels. Table 5 shows the cut-flow for the signal benchmark points after S1, S2, and S3. After S2, we see that the background is comparable (or larger) than the signal in both the channels. However, implementing S3 reduces the background

S2	H_T	L_T	$L_T + p_T^{\text{miss}}$	S_T
low-mass	>200	>200	>400	>700
mid-mass	>200	>200	>500	>800
high-mass	>400	>400	>700	>1100

Table 4: The selections implemented in S2 for the signal and background processes in the 3L1F_j final state. The selections are shown in units of GeV.

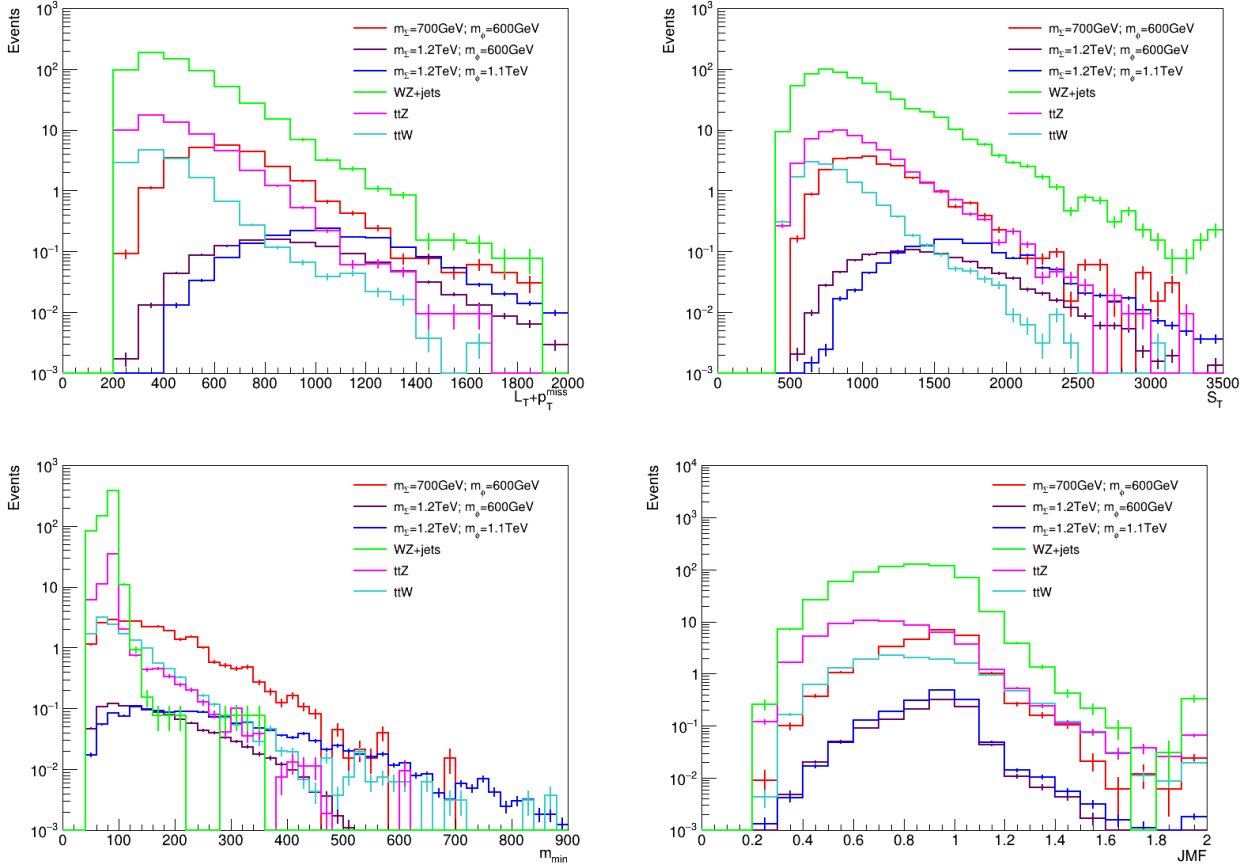


Figure 7: The distributions of $L_T + p_T^{\text{miss}}$, S_T (top row) and m_{\min} , JMF (bottom row) are shown for signal and background processes after the S1 selections are imposed in the 3L1F_j final state.

significantly. The signal yield in the 3L1F_j channel is smaller than in the 2L2F_j channel for the low-mass benchmark point.

The sensitivity of the signal is typically calculated with the formula: $Z_{\text{simple}} = \frac{s}{\sqrt{b}}$ where s is the number of signal events and b is the number of background events. This can overestimate the significance in cases where the background is very small. We instead adopt the general formula [64, 65] to calculate the significance, which also permits incorporating the uncertainty in the background measurements. The general formula is

$$Z_{\text{general}} = \left[2 \left((s + b) \ln \left[\frac{(s + b)(b + \Delta_b^2)}{b^2 + (s + b)\Delta_b^2} \right] - \frac{b^2}{\Delta_b^2} \ln \left[1 + \frac{s\Delta_b^2}{b(b + \Delta_b^2)} \right] \right) \right]^{1/2}. \quad (14)$$

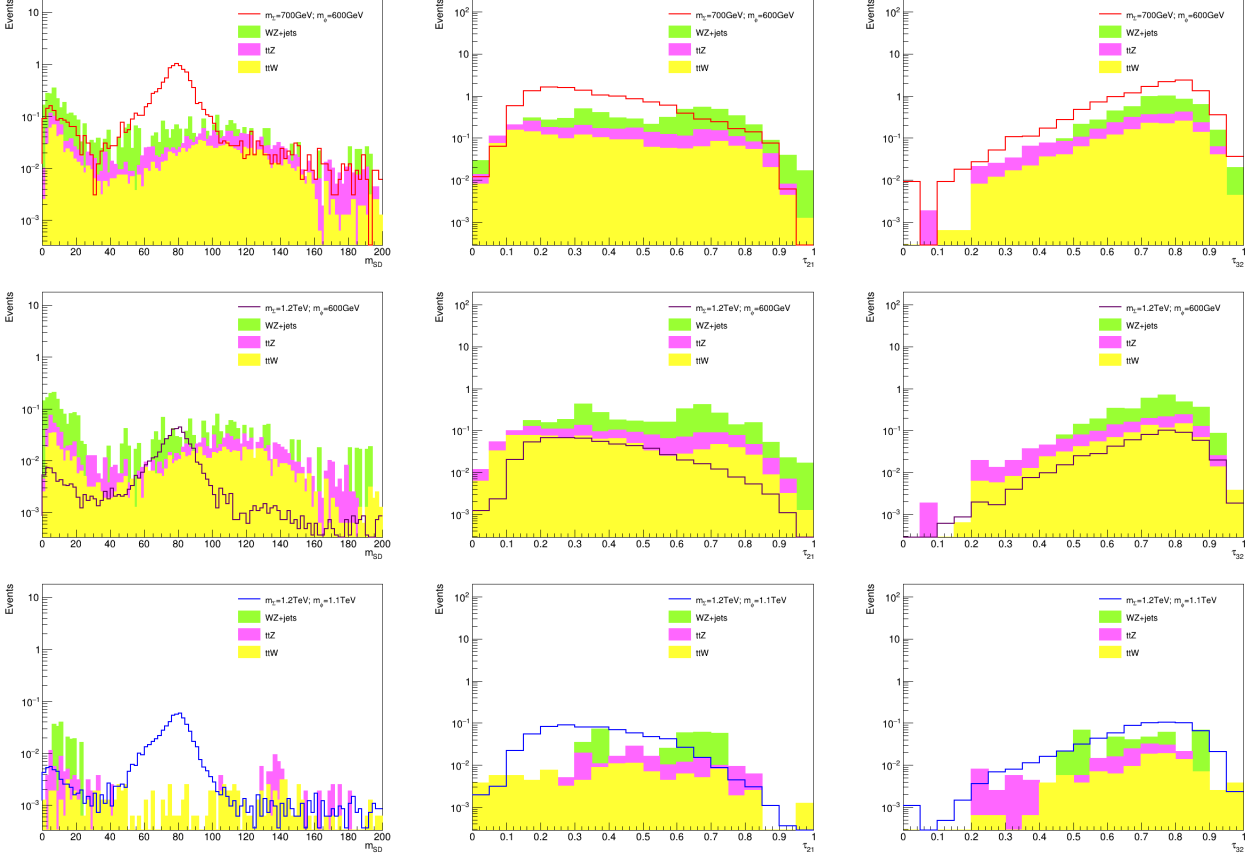


Figure 8: The jet substructure variables for the low-mass (top), med-mass (middle), and high-mass (bottom) benchmark point and the background processes after the S2 selections are imposed in the 3L1F_j final state.

where, Δ_b is the uncertainty in the background estimation. In Table 6 we have tabulated the significance using the general form with two choices of background uncertainty, $\Delta_b = 10\%$ and 50% . For comparison we also tabulate the significance Z_{simple} . The significance is calculated at current and projected future luminosities of the LHC.

We can see from Table 6 that the low-mass benchmark point has the largest significance in both the channels. The significance in the low-mass point is more than 5σ at the current luminosity of the LHC experiments, when no uncertainty in the background is assumed. However, with a background uncertainty $\Delta_b = 50\%$, significance more than 5σ is achievable at 300 fb^{-1} only in the 3L1F_j channel. The significance in the 2L2F_j channel is comparatively less because the signal and background yields are comparable. If we consider the high mass point, then the significance in both the channels is almost similar. However with $\Delta_b = 50\%$, the 3L1F_j channel offers a significance of more than 5σ with an integrated luminosity of 3000 fb^{-1} . Overall we found that the performance of both the channels is excellent in the low-mass and high-mass benchmark points and both of these channels show potential for discovery (or stringent constraints) from current and future luminosities at the LHC experiments.

Final State	$m_{\Sigma^{++}}, m_{\phi^{++}}$ (GeV)	Cut Flow ($\times 10^{-3}$ fb)					
		S1		S2		S3	
		Sig	Bkg	Sig	Bkg	Sig	Bkg
2L2F _j	1200,1100 (high-mass)	47.1	51530	32.2	669.1	18.33	7.28
	1200,600 (med-mass)	28.1	51530	18.5	1506	9.36	9.74
	700,600 (low-mass)	613.8	51530	390.5	6592	208.50	182.60
3L1F _j	1200,1100 (high-mass)	11.5	5096	4.98	3.05	3.65	0.12
	1200,600 (med-mass)	8.2	5096	3.97	24.66	2.82	4.48
	700,600 (low-mass)	184.4	5096	86.90	39.01	65.20	7.33

Table 5: The cut flow for the 2L2F_j and 3L1F_j final states for the different sets of selections applied.

Final State	$m_{\Sigma^{++}}, m_{\phi^{++}}$ (GeV)	Z_{simple}	Z_{general}	
			$\Delta_b = 10\%$	$\Delta_b = 50\%$
2L2F _j	1200,1100 (high-mass)	2.53 (3.72) [11.78]	1.94 (2.84) [7.85]	1.65 (2.11) [2.99]
	1200,600 (med-mass)	1.12 (1.64) [5.20]	0.98 (1.42) [3.912]	0.82 (1.05) [1.44]
	700,600 (low-mass)	5.73 (8.45) [26.72]	4.30 (5.59) [8.15]	1.64 (1.70) [1.74]
3L1F _j	1200,1100 (high-mass)	3.90 (5.76) [18.20]	1.60 (2.36) [7.41]	1.59 (2.31) [6.28]
	1200,600 (med-mass)	0.50 (0.73) [2.31]	0.45 (0.66) [1.96]	0.42 (0.57) [0.95]
	700,600 (low-mass)	8.95 (13.19) [41.72]	5.21 (7.56) [19.74]	4.13 (5.14) [6.91]

Table 6: The significance of 2L2F_j and 3L1F_j channels calculated at integrated luminosities of 138, (300) and [3000] fb^{-1} including two estimates of uncertainties in background yield.

5 Outlook

To address the shortcomings of the standard model, extensions beyond the SM introduce new physics at or beyond the TeV scale, often including new particles. Scenarios involving both fermion and

scalar multiplets naturally arise in several BSM theories like composite Higgs models or grand unified theories. Such scenarios can lead to unique collider signatures depending on the mass hierarchies between the new hypothetical particles. In this paper we focused on a simplified model with a neutral fermion quintuplet and a scalar quadruplet, which can generate neutrino masses through tree and loop-level processes. The quintuplet fermions decay into standard model gauge bosons via the scalars and produce distinctive signals at the LHC involving multilepton and multijet final states.

These final states can often have comparatively large SM backgrounds at the LHC given the low production cross sections of the new fermions, especially at around 1 TeV or higher fermion masses. This work examined the pair production of quintuplet fermions in the range (700 -1200) GeV, whose decay eventually yields highly boosted W and Z bosons. Here we focused on production of doubly charged fermions due to their higher cross sections over other pair production channels. We used fatjets to target the boosted gauge boson decays, and applied advanced jet substructure techniques and dedicated variables to improve the LHC sensitivity in two specific final states: $2\text{L}2\text{F}_j$ and $3\text{L}1\text{F}_j$.

We did detailed analysis of optimizing the signal selection against backgrounds for three benchmark scenarios with low, medium, and high masses of the quintuplet fermions and scalars. A well chosen selection strategy ensured a high sensitivity to the signal over the background for the different mass scenarios. We found that the low-mass scenario achieved the highest significance in both the $2\text{L}2\text{F}_j$ and $3\text{L}1\text{F}_j$ channels, exceeding 5σ at current LHC luminosity with no background uncertainty. With a conservative choice of 50% background uncertainty, only the $3\text{L}1\text{F}_j$ channel reaches $\geq 5\sigma$ at 3000 fb^{-1} . For the high-mass scenario, the significance is similar for the two channels with no background uncertainty. In the conservative case of 50% background uncertainty, here as well the $3\text{L}1\text{F}_j$ channel has $\geq 5\sigma$ significance with 3000 fb^{-1} .

Both channels maintain good sensitivity with a realistic background uncertainty, and will enable the LHC experiments to probe masses of more than 1 TeV even with the existing LHC dataset of 300 fb^{-1} (Run 2 + Run 3), and higher masses with the projected future luminosities of HL-LHC.

Acknowledgments

N.K. would like to thank Anusandhan National Research Foundation Government of India for the support from Core Research Grant with grant agreement number CRG/2022/004120.

References

- [1] P.A. Zyla et al. Review of Particle Physics. *PTEP*, 2020(8):083C01, 2020.
- [2] B. Abi et al. Measurement of the Positive Muon Anomalous Magnetic Moment to 0.46 ppm. *Phys. Rev. Lett.*, 126(14):141801, 2021.
- [3] David London and Joaquim Matias. B Flavour Anomalies: 2021 Theoretical Status Report. *Ann. Rev. Nucl. Part. Sci.*, 72:37–68, 2022.
- [4] J. A. Aguilar-Saavedra, R. Benbrik, S. Heinemeyer, and M. Pérez-Victoria. Handbook of vector-like quarks: Mixing and single production. *Phys. Rev. D*, 88(9):094010, 2013.
- [5] Nilanjana Kumar and Stephen P. Martin. Vectorlike Leptons at the Large Hadron Collider. *Phys. Rev. D*, 92(11):115018, 2015.

- [6] John Kearney, Aaron Pierce, and Neal Weiner. Vectorlike Fermions and Higgs Couplings. *Phys. Rev. D*, 86:113005, 2012.
- [7] Robert Foot, H. Lew, X. G. He, and Girish C. Joshi. Seesaw Neutrino Masses Induced by a Triplet of Leptons. *Z. Phys. C*, 44:441, 1989.
- [8] Takaaki Nomura and Hiroshi Okada. Neutrino mass with large $SU(2)_L$ multiplet fields. *Phys. Rev. D*, 96(9):095017, 2017.
- [9] Nilanjana Kumar, Takaaki Nomura, and Hiroshi Okada. Scotogenic neutrino mass with large $SU(2)_L$ multiplet fields. *Eur. Phys. J. C*, 80(8):801, 2020.
- [10] K. S. Babu, S. Nandi, and Zurab Tavartkiladze. New Mechanism for Neutrino Mass Generation and Triply Charged Higgs Bosons at the LHC. *Phys. Rev. D*, 80:071702, 2009.
- [11] Avinanda Chaudhuri, Walter Grimus, and Biswarup Mukhopadhyaya. Doubly charged scalar decays in a type II seesaw scenario with two Higgs triplets. *JHEP*, 02:060, 2014.
- [12] Yong Du, Aaron Dunbrack, Michael J. Ramsey-Musolf, and Jiang-Hao Yu. Type-II Seesaw Scalar Triplet Model at a 100 TeV pp Collider: Discovery and Higgs Portal Coupling Determination. *JHEP*, 01:101, 2019.
- [13] H. Georgi and S. L. Glashow. Unity of All Elementary Particle Forces. *Phys. Rev. Lett.*, 32:438–441, 1974.
- [14] G. Senjanovic and Rabindra N. Mohapatra. Exact Left-Right Symmetry and Spontaneous Violation of Parity. *Phys. Rev. D*, 12:1502, 1975.
- [15] Sanjib Kumar Agarwalla, Kirtiman Ghosh, and Ayon Patra. Sub-TeV Quintuplet Minimal Dark Matter with Left-Right Symmetry. *JHEP*, 05:123, 2018.
- [16] Ian Low, Witold Skiba, and David Tucker-Smith. Little Higgses from an antisymmetric condensate. *Phys. Rev. D*, 66:072001, 2002.
- [17] Natascia Vignaroli. Discovering the composite Higgs through the decay of a heavy fermion. *JHEP*, 07:158, 2012.
- [18] Yi Cai and Michael A. Schmidt. Revisiting the $R\nu$ MDM Models. *JHEP*, 05:028, 2016.
- [19] Shruti Dubey, Nilanjana Kumar, Tanumoy Mandal, Subhadip Mitra, and Rachit Sharma. Vectorlike τ production through leptoquarks. 8 2025.
- [20] Saiyad Ashanujjaman, Debajyoti Choudhury, and Kirtiman Ghosh. Search for exotic leptons in final states with two or three leptons and fat-jets at 13 TeV LHC. *JHEP*, 04:150, 2022.
- [21] Nilanjana Kumar and Vandana Sahdev. Exotic Decays and Collider Signatures of pNGB Scalars in the $SU(5)/SO(5)$ Composite Higgs Model. 3 2025.
- [22] Avik Banerjee et al. Phenomenological aspects of composite Higgs scenarios: exotic scalars and vector-like quarks. 3 2022.
- [23] Teng Ma, Bin Zhang, and Giacomo Cacciapaglia. Doubly Charged Lepton from an Exotic Doublet at the LHC. *Phys. Rev. D*, 89(9):093022, 2014.
- [24] Nilanjana Kumar and Vandana Sahdev. Alternative signatures of the quintuplet fermions at the LHC and future linear colliders. *Phys. Rev. D*, 105(11):115016, 2022.

[25] Georges Aad et al. Search for type-III seesaw heavy leptons in leptonic final states in pp collisions at $\sqrt{s} = 13$ TeV with the ATLAS detector. *Eur. Phys. J. C*, 82(11):988, 2022.

[26] Armen Tumasyan et al. Inclusive nonresonant multilepton probes of new phenomena at $\sqrt{s}=13$ TeV. *Phys. Rev. D*, 105(11):112007, 2022.

[27] G. Abbiendi et al. Search for Charged Higgs bosons: Combined Results Using LEP Data. *Eur. Phys. J. C*, 73:2463, 2013.

[28] Georges Aad et al. Search for resonant WZ production in the fully leptonic final state in proton–proton collisions at $\sqrt{s} = 13$ TeV with the ATLAS detector. *Eur. Phys. J. C*, 83(7):633, 2023.

[29] Albert M Sirunyan et al. Search for charged Higgs bosons produced in vector boson fusion processes and decaying into vector boson pairs in proton–proton collisions at $\sqrt{s} = 13$ TeV. *Eur. Phys. J. C*, 81(8):723, 2021.

[30] Georges Aad et al. Measurement and interpretation of same-sign W boson pair production in association with two jets in pp collisions at $\sqrt{s} = 13$ TeV with the ATLAS detector. *JHEP*, 04:026, 2024.

[31] Georges Aad et al. Search for doubly charged Higgs boson production in multi-lepton final states using 139 fb^{-1} of proton–proton collisions at $\sqrt{s} = 13$ TeV with the ATLAS detector. *Eur. Phys. J. C*, 83(7):605, 2023.

[32] Albert M Sirunyan et al. Search for charged Higgs bosons in the $H^\pm \rightarrow \tau^\pm \nu_\tau$ decay channel in proton-proton collisions at $\sqrt{s} = 13$ TeV. *JHEP*, 07:142, 2019.

[33] Arindam Das and Sanjoy Mandal. Bounds on the triplet fermions in type-III seesaw and implications for collider searches. *Nucl. Phys. B*, 966:115374, 2021.

[34] You Yu, Chong-Xing Yue, and Shuo Yang. Signatures of the quintuplet leptons at the LHC. *Phys. Rev. D*, 91(9):093003, 2015.

[35] Chian-Shu Chen and Ya-Juan Zheng. LHC signatures for the cascade seesaw mechanism. *PTEP*, 2015:103B02, 2015.

[36] A. Ozansoy. Doubly Charged Lepton Search Potential of the FCC-Based Energy-Frontier Electron-Proton Colliders. *Adv. High Energy Phys.*, 2020:9234130, 2020.

[37] Yu-Chen Guo, Chong-Xing Yue, and Zhi-Cheng Liu. The signatures of doubly charged leptons in future linear colliders. *J. Phys. G*, 44(8):085004, 2017.

[38] Qing-Guo Zeng. Production of the quintuplet leptons in future high energy linear $e + e -$ colliders. *Nucl. Phys. B*, 905:251–263, 2016.

[39] Debajyoti Choudhury, Kuldeep Deka, and Nilanjana Kumar. Looking for a vectorlike B quark at the LHC using jet substructure. *Phys. Rev. D*, 104(3):035004, 2021.

[40] Saiyad Ashanujjaman and Kirtiman Ghosh. Type-III see-saw: Search for triplet fermions in final states with multiple leptons and fat-jets at 13 TeV LHC. *Phys. Lett. B*, 825:136889, 2022.

[41] Atri Dey, Rafiqul Rahaman, and Santosh Kumar Rai. Fatjet signatures of heavy neutrinos and heavy leptons in a left-right model with universal seesaw at the HL-LHC. *Eur. Phys. J. C*, 84(2):132, 2024.

[42] Nilanjana Kumar. A Brief Review on Jet Substructure in Connection with Collider Phenomenology. 11 2022.

[43] Aneesh Manohar, Paolo Nason, Gavin Salam, and Giulia Zanderighi. The photon parton distribution function: updates and applications. In *International Congress of Basic Science*, 8 2024.

[44] Stefano Carrazza. Towards the determination of the photon parton distribution function constrained by LHC data. *PoS*, DIS2013:279, 2013.

[45] Richard D. Ball, Valerio Bertone, Stefano Carrazza, Luigi Del Debbio, Stefano Forte, Alberto Guffanti, Nathan P. Hartland, and Juan Rojo. Parton distributions with QED corrections. *Nucl. Phys. B*, 877:290–320, 2013.

[46] J. Alwall, R. Frederix, S. Frixione, V. Hirschi, F. Maltoni, O. Mattelaer, H. S. Shao, T. Stelzer, P. Torrielli, and M. Zaro. The automated computation of tree-level and next-to-leading order differential cross sections, and their matching to parton shower simulations. *JHEP*, 07:079, 2014.

[47] R. Frederix, S. Frixione, V. Hirschi, D. Pagani, H. S. Shao, and M. Zaro. The automation of next-to-leading order electroweak calculations. *JHEP*, 07:185, 2018. [Erratum: *JHEP* 11, 085 (2021)].

[48] Andy Buckley et al. LHAPDF6: parton density access in the LHC precision era. *The European Physical Journal C*, 75(3):132, Mar 2015.

[49] Measurement of top quark pair production in association with a Z boson in proton-proton collisions at $\sqrt{s} = 13$ TeV. 2019.

[50] A. M. Sirunyan et al. Observation of the Production of Three Massive Gauge Bosons at $\sqrt{s} = 13$ TeV. *Phys. Rev. Lett.*, 125:151802, Oct 2020.

[51] A. Tumasyan et al. Measurement of differential $t\bar{t}$ production cross sections in the full kinematic range using lepton + jets events from proton-proton collisions at $\sqrt{s} = 13$ TeV. *Phys. Rev. D*, 104:092013, Nov 2021.

[52] Georges Aad et al. Measurements of $W^+W^- + \geq 1$ jet production cross-sections in pp collisions at $\sqrt{s} = 13$ TeV with the ATLAS detector. *JHEP*, 06:003, 2021.

[53] Aram Hayrapetyan et al. Measurement of differential $ZZ + \text{jets}$ production cross sections in pp collisions at $\sqrt{s} = 13$ TeV. *JHEP*, 10:209, 2024.

[54] Armen Tumasyan et al. Measurement of the cross section of top quark-antiquark pair production in association with a W boson in proton-proton collisions at $\sqrt{s} = 13$ TeV. *JHEP*, 07:219, 2023.

[55] Christian Bierlich et al. A comprehensive guide to the physics and usage of PYTHIA 8.3. *SciPost Phys. Codebases*, page 8, 2022.

[56] Christian Bierlich et al. Codebase release 8.3 for PYTHIA. *SciPost Phys. Codebases*, pages 8–r8.3, 2022.

[57] Matteo Cacciari, Gavin P. Salam, and Gregory Soyez. The anti- k_t jet clustering algorithm. *JHEP*, 04:063, 2008.

[58] Matteo Cacciari, Gavin P. Salam, and Gregory Soyez. FastJet User Manual. *Eur. Phys. J. C*, 72:1896, 2012.

- [59] J. de Favereau et al. DELPHES 3: a modular framework for fast simulation of a generic collider experiment. *Journal of High Energy Physics*, 2014(2):57, Feb 2014.
- [60] Andrew J. Larkoski, Simone Marzani, Gregory Soyez, and Jesse Thaler. Soft drop. *Journal of High Energy Physics*, 2014(5):146, May 2014.
- [61] Stephen D. Ellis, Christopher K. Vermilion, and Jonathan R. Walsh. Recombination algorithms and jet substructure: Pruning as a tool for heavy particle searches. *Phys. Rev. D*, 81:094023, May 2010.
- [62] Davide Napoletano and Gregory Soyez. Computing N-subjettiness for boosted jets. *Journal of High Energy Physics*, 2018(12):31, Dec 2018.
- [63] G. Aad et al. Measurement of soft-drop jet observables in pp collisions with the ATLAS detector at $\sqrt{s} = 13$ TeV. *Phys. Rev. D*, 101:052007, Mar 2020.
- [64] Glen Cowan, Kyle Cranmer, Eilam Gross, and Ofer Vitells. Asymptotic formulae for likelihood-based tests of new physics. *Eur. Phys. J. C*, 71:1554, 2011. [Erratum: Eur.Phys.J.C 73, 2501 (2013)].
- [65] Robert D. Cousins, James T. Linnemann, and Jordan Tucker. Evaluation of three methods for calculating statistical significance when incorporating a systematic uncertainty into a test of the background-only hypothesis for a Poisson process. *Nucl. Instrum. Meth. A*, 595(2):480–501, 2008.